Facile Synthesis of Graphite/PEDOT/MnO$_2$ Composites on Commercial Supercapacitor Separator Membranes as Flexible and High-Performance Supercapacitor Electrodes

Pengyi Tang,[†] Lijuan Han,[†,‡] and Li Zhang*,[†,‡]

[†]Department of Mechanical and Automation Engineering, The Chinese University of Hong Kong, Hong Kong SAR, People's Republic of China

[‡]Shun Hing Institute of Advanced Engineering, The Chinese University of Hong Kong, Hong Kong SAR, People's Republic of China

S Supporting Information

ABSTRACT: A facile and low-cost method is presented to synthesize graphite/PEDOT/MnO$_2$ composites with controlled network structures on commercial supercapacitor separator (CSS) membranes for high-performance supercapacitors, in which pencil lead and a cellulose-based commercial supercapacitor separator membrane were applied as the graphite source and the flexible substrate, respectively. The dependence of PEDOT and MnO$_2$ loading on the structural formation, the electrochemical performance of the hybrid electrode, and the formation mechanism of MnO$_2$ nanowires are systematically investigated. The optimized electrode possesses a high areal capacitance of 316.4 mF/cm^2 at a scan rate of 10 mV/s and specific capacitance of 195.7 F/g at 0.5 A/g. The asymmetric supercapacitor device assembled using optimized CSS/Graphite/PEDOT/MnO$_2$ electrode and activated carbon electrode exhibits a high energy density of 31.4 Wh/kg at a power density of 90 W/kg and maintains 1 Wh/kg at 4500 W/kg. After 2000 cycles, the device retains 81.1% of initial specific capacitance, and can drive a mini DC-motor for ca. 10 s. The enhanced capability of the CSS-based graphite/PEDOT/MnO$_2$ network electrode has high potential for low-cost, high-performance, and flexible supercapacitors.

KEYWORDS: commercial supercapacitor separator, graphite, PEDOT, MnO$_2$, flexible supercapacitor
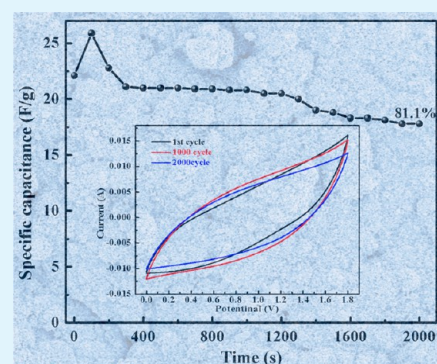
1. INTRODUCTION

Owing to the tremendous increase in energy consumption in modern society, the development of sustainable and renewable energy sources is urgently required.[1,2] As an energy storage device, supercapacitors (SCs) possess higher energy density than traditional electrostatic capacitors and deliver much higher power density than batteries.[3,4] Among various configurations of SCs, planar ones have shown great promise in upcoming next-generation portable and flexible electronics such as roll-up displays, photovoltaic cells, and wearable devices.[5−10] In addition, planar SCs are feasible in realizing compact-device-designs by stacking, and are capable of performing fast transport of ion due to their advantages of thickness, mechanical flexibility, and lightweight.[11−16]

Recently, researchers have reported the fabrication of flexible planar electrodes by direct deposition of electroactive nano-materials on two-dimensional flexible substrates, including Au thin films,[1] Ti foil,[11] carbon cloth,[17] lens wiping paper,[18] plastics,[19] commercially available photo papers,[20] etc. Among them, cellulose papers represent the state-of-the-art as a flexible substrate for planar electrodes because of their excellent mechanical strength, high flexibility, and low cost.[4,21−27] For instance, Cui et al. designed flexible supercapacitors based on commercial paper using printing and solvent-free drawing

methods;[24,25] the pencil-drawing-assistant paper-based super-capacitor exhibited superior cycling performance and an areal capacitance of 2.3 mF/cm^2.[25] Meanwhile, Wang et al. adopted Au as the intermediate conductive layer to synthesize polyaniline (PANI)/Au/paper composite and obtained an ultrahigh areal capacitance of 0.8 F/cm^2 at 1 mA/cm^2.[1] More recently, Chen et al. combined pencil-drawing with electro-deposition technology to fabricate graphite/PANI hybrid electrodes on commercially printed paper which showed a high areal capacitance of 355.6 mF/cm^2 at a current density of 0.5 mA/cm^2.[27] The performance of these planar paper-based SCs, however, suffers from the poor reaction kinetics and drastic volume variation during an electrolyte ions insertion/extraction process, which is expected to be improved via designing three-dimensional (3D) nanostructural architecture of pseudocapacitive materials on the surface of the electrode.

Among the available pesudocapacitive materials, MnO$_2$, an important member of the metal oxide family, has been regarded as a promising candidate due to its high theoretical capacitance (1370 F/g), as well as nontoxicity, abundance, low-cost, and

environmental benignity. Ivey et al. demonstrated that the morphologies of electrodeposited MnO_2 are controlled by different nucleation mechanisms: i.e., the progressive nucleation mechanisms, the mix of instantaneous/progressive nucleation and the instantaneous nucleation.[28] By applying superior conductive materials, such as poly(3,4-ethylene dioxythiophene) (PEDOT) and Au/Pt nanoparticles as the interfaces between conductive substrate and pseudocapacitive material, the nucleation mechanisms and morphology of MnO_2 material can be tuned in a controlled fashion.[29−31] For example, Li et al. reported that the introduction of PEDOT species on the graphene sheets induced the formation of ordered MnO_2 nanowires because of the matched chemical bond of PEDOT and MnO_2 species.[29] Xu et al. revealed that the decoration of noble metallic (i.e., Au, Pd, or Pt) nanoparticles on nickel foam tuned the nucleation mechanisms of MnO_2 species and resulted in the formation of MnO_2 nanosheets array.[31] To date, however, it is still a great challenge to design well-defined 3D nanostructures for planar flexible SCs with high energy storage capacity and superior cycling stability.[10]

Herein, we report the preparation of graphite/PEDOT/MnO_2 composites with networked hybrid nanostructures on commercial supercapacitor separator (CSS) membranes. The strategy for synthesizing CSS/G/PEDOT/MnO_2 composite is schematically depicted in Figure 1. In particular, pencil-drawing
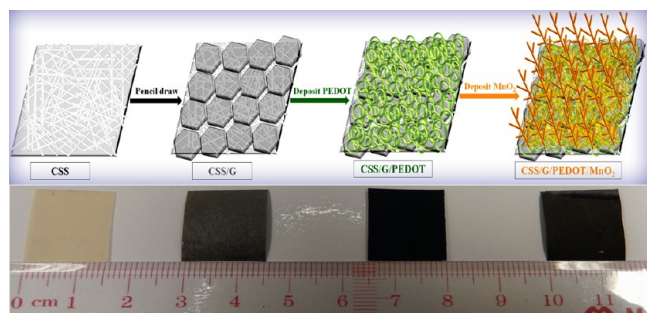

Figure 1. Schematic illustration of the processing procedure of a CSS/G/PEDOT/MnO_2 electrode.

and electrochemical deposition methods are applied to deposit graphite, PEDOT, and MnO_2 species; the dependence of PEDOT and MnO_2 mass loading on the structural evolution and electrochemical properties of the hybrid electrode is systematically investigated. The main advantages of the optimized CSS/G/PEDOT/MnO_2 hybrid electrode design are listed as follows: (i) the lightweight (5.3 mg/cm^2) and highly porous CSS membrane serves as the flexible substrate, allowing rapid diffusion of electrolyte ion; (ii) the bottom graphite layer provides initial electrical conductivity; (iii) the intermediate porous PEDOT layer significantly enhances the conductivity of the electrode and induces the formation of MnO_2 nanowires; (iv) the intercrossed MnO_2 nanowires provide large surface area, which greatly increase the electroactive surface area and thus enhance the electrochemical performance of the electrode.

2. EXPERIMENTAL SECTION

2.1. Chemicals and Materials. $Mn(CH_3COO)_2$ (analytically pure), 3,4-Ethelenedixythiophene (EDOT, 99% mass fraction), sodium dodecyl sulfate (SDS, analytically pure), $LiClO_4$ (analytically pure), and Na_2SO_4 (analytically pure) were purchased from Aladdin Reagent Co. Ltd. Activated carbon (AC, TF-B520) was obtained from

Shanghai Carbosino Material Co., Ltd. with a specific surface area of 2000 ($\pm$100) m^2/g. A commercial supercapacitor separator (DR2012 type) was purchased from Suzhou Beige New Materials & Technology Co. Ltd..

2.2. Preparation of the Electrodes. *2.2.1. CSS/Graphite/PEDOT/MnO_2 Hybrid Electrodes.* CSS membrane was used as the supporting substrate for G/PEDOT/MnO_2 ternary composite. Before electrochemical deposition, a piece of CSS membrane with a typical area of about 2 × 1.5 cm^2 was immersed into 0.3 M hydrochloric acid aqueous solution for 10 min, washed with deionized water thoroughly to remove foaming composition, and placed in a fume hood at room temperature for drying. Afterward, a commercial 9B pencil was used to draw on the surface of acid-treated CSS five times, forming a uniform graphite layer (with mass loading of approximate 1.6 mg/cm^2). And then, PEDOT and MnO_2 were electrodeposited on the previously obtained CSS/G substrate sequentially based on previous reports.[31,32] The detailed steps were as follows: first, the PEDOT nanoporous networks were synthesized by oxidation of EDOT (aqueous solution of 80 mM EDOT, 100 mM $LiClO_4$, and 140 mM SDS) at a constant potential of 1.0 V vs saturated calomel electrode (SCE). After that, MnO_2 nanowires were deposited at a constant potential of 1.0 V vs SCE in the aqueous solution of 0.5 M $Mn(CH_3COO)_2$. Finally, the obtained hybrid electrode was washed with deionized water several times, and then it was heat-treated at 100 °C for 2 h. All the electrochemical deposition was conducted by a CHI 660E electrochemical workstation with a three-electrode cell consisting of an SCE as the reference electrode, a platinum plate (2.0 × 2.0 cm^2) as the counter electrode and the treated CSS (active area: 2 × 1.5 cm^2) as the working electrode. The mass of total active material (PEDOT: 2.4 mg + MnO_2: 0.9 mg) of the optimized hybrid electrode was about 3.3 mg (i.e., 1.1 mg/cm^2), which is measured by a microbalance.

2.2.2. Activated Carbon (AC) Electrode. Nickel foam was treated with acetone and hydrochloric acid to clean and etch the surface. The AC, acetylene black, and poly(tetrafluoroethylene) (PTFE) were mixed in a mass ratio of 85:10:5, and dispersed in ethanol to produce a homogeneous paste. Finally, the resulting mixture was pasted onto the treated nickel foam (2 × 1.5 cm^2) with a spatula. Then, the fabricated electrode was pressed and dried overnight under vacuum at 80 °C.

2.3. Assembly of an Asymmetric Supercapacitor. For the construction of an asymmetric supercapacitor device, CSS/G/PEDOT/MnO_2 and AC electrodes were used as the positive and the negative electrodes, respectively; and another piece of CSS membrane is employed as the supercapacitor separator. The mass ratio of negative electrode (AC: 2.4 mg) to positive electrode (CSS/G/PEDOT/MnO_2: 3.3 mg) was fixed to 0.73:1, which was based on charge balance theory[33] and their individual specific capacitances in 0.5 M Na_2SO_4 aqueous solution (199 F/g vs 147 F/g at a scan rate of 50 mV/s).

2.4. Microstructural Properties Characterization of the Samples. The as-synthesized samples were characterized using X-ray powder diffraction (XRD; Rigaku RU-300 diffractometer; monochromated Cu Kα1 radiation, λ = 1.540 598 1 Å; 60.0 kV, 30.0 mA), Raman spectroscopy (RM-1000 Micro Raman Spectrometer, light source: 514 nm), Fourier-transform infrared spectroscopy (FT-IR), X-ray photoelectron spectroscopy (XPS, Escalab 250Xi), field emission scanning electron microscope (SEM, S-360, Cambridge), transmission electron microscopy (TEM, Tecnai F20, FEI), and X-ray energy dispersive spectrometer (EDS). The TEM specimen was prepared by the following procedure: hybrid electrode was cut into pieces with scissors, and then suspended in ethanol with ultrasonic vibration for 5 min to strip off the PEDOT/MnO_2 network nanocomposites. And then a drop of the suspension was transferred onto a standard copper TEM grid covered by carbon film.

2.5. Electrochemical Properties Measurement. The electrochemical performance of CSS/G/PEDOT/MnO_2 hybrid electrodes and the corresponding asymmetric supercapacitor was characterized using cyclic voltammetry (CV), galvanostatic charge−discharge, and electrochemical impedance spectroscopy (EIS, recorded at open circuit potential with amplitude of 5 mV in the frequency range of 10^{-2}−10^5 Hz) techniques on a CHI 660E electrochemical workstation
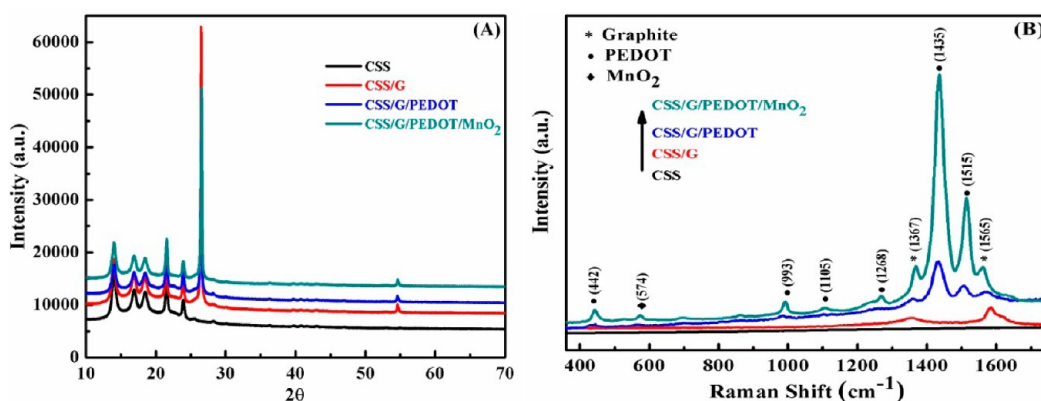
10507

dx.doi.org/10.1021/am5021028 | *ACS Appl. Mater. Interfaces* 2014, 6, 10506−10515

Figure 2. XRD and Raman spectrum of CSS, CSS/G, CSS/G/PEDOT, and CSS/G/PEDOT/MnO$_2$: (A) XRD spectra; (B) Raman spectra.

at ambient temperature. All the measurements were carried out in a 0.5 M Na$_2$SO$_4$ aqueous solution. In the three-electrode system, a Pt foil of 2.0 × 2.0 cm^2 and an SCE were applied as the counter and reference electrodes, respectively. The specific capacitance measured by chronopotentiometry was calculated according to the equation as follows:

$$C_{sp} = I \times \Delta t/(\Delta V \times m) \qquad (1)$$

where C_{sp} (F/g) is the specific capacitance of the electrode (C_{sp-s}) or asymmetric supercapacitor (C_{sp-d}), I (A) the constant discharging current, Δt (s) the discharging time, ΔV (V) the potential drop at a constant discharge current, and m (g) the mass of a single electrode or the total active material mass of positive and negative electrodes.

The energy (E, Wh/kg) and power densities (P, W/kg) of a supercapacitor is expressed by following equations:

$$E = \frac{C_{sp-d}\Delta V^2}{2}, \quad P = \frac{\Delta VI}{2m} \qquad (2)$$

where C_{sp-d} (F/g), ΔV (V), I (A) and m (g) are the specific capacitance of the supercapacitor, the potential window of discharge current and the total active material mass of positive and negative electrodes, respectively.

3. RESULTS AND DISCUSSION

The crystallographic structure of the as-prepared hybrid electrodes is examined by XRD as shown in Figure 2A. The four peaks at around 14.0°, 16.9°, 18.4°, 21.5°, and 24.0° could be assigned to the diffractogram of typical cellulose *I* crystalline structure.[34] Accordingly, the CSS membrane composed by cellulose *I* crystalline structure has the advantage of low coefficient of thermal expansion (CTE), high mechanical strength, and excellent flexibility.[35] And the peaks at 26.5° and 54.6° imply the presence of graphite species in the CSS/G, CSS/G/PEDOT and CSS/G/PEDOT/MnO$_2$ hybrid electrodes.[36] The curve of CSS/G/PEDOT/MnO$_2$ hybrid electrode, however, does not display any visible diffraction peaks corresponding to MnO$_2$, revealing the amorphous phase of MnO$_2$ in the ternary composite. In order to further understand the microstructure of MnO$_2$ and PEDOT species, Raman microscopy, which is sensitive to the short-range order structure in amorphous materials, was utilized. As shown in Figure 2B, none of the Raman spectrum of CSS electrodes exhibits visible peaks, while the peaks at 1367, 1565, and 442 cm^{-1}; 993, 1105, 1268, 1435, and 1515 cm^{-1} corresponding to the graphite and PEDOT in hybrid electrodes, repectively. And the weak peak at 574 cm^{-1} demonstrates the existence of MnO$_2$ species in the CSS/G/PEDOT/MnO$_2$ electrode.[31,32] These results are in accordance with the FT-IR test in Supporting
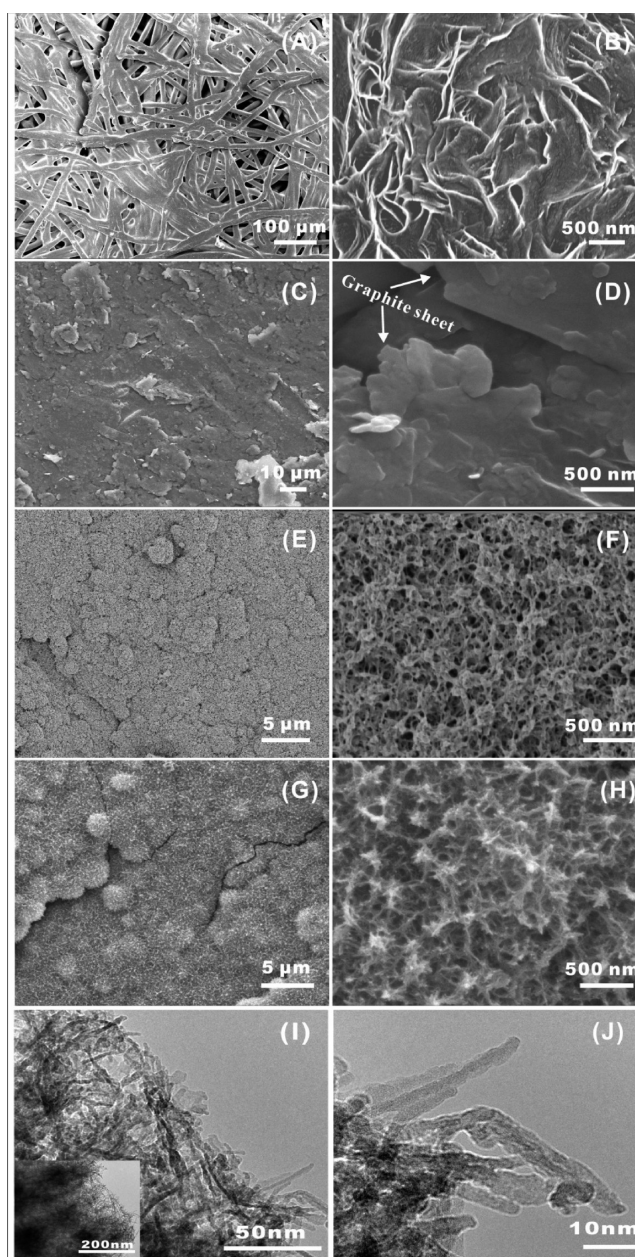

Figure 3. (A−H) SEM images of CSS (A and B), CSS/G (C and D), CSS/G/PEDOT (E and F), and CSS/G/PEDOT/MnO$_2$ (G and H); and (I−J) TEM images of CSS/G/PEDOT/MnO$_2$.
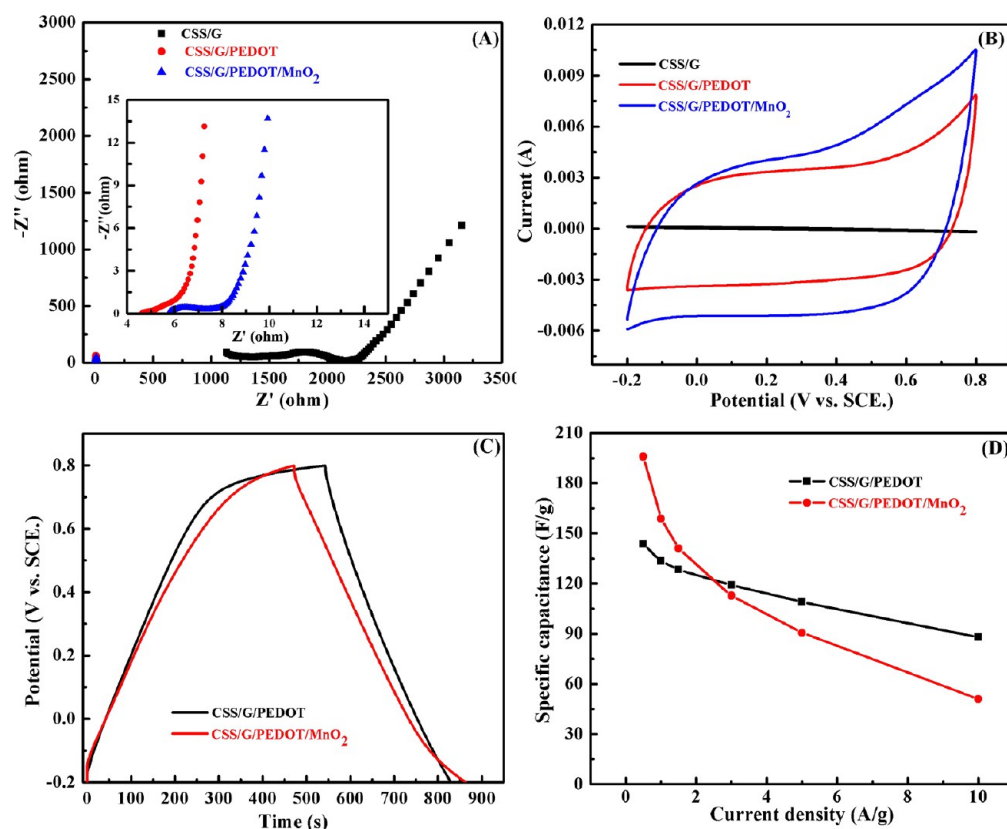
Figure 4. Electrochemical properties of CSS/G, CSS/G/PEDOT, and CSS/G/PEDOT/MnO$_2$ with 2 C MnO$_2$ deposition electrodes: (A) Nyquist plots, (B) CV curves at a scan rate of 10 mV/s, (C) the galvanostatic charge−discharge curves at a current density of 0.5 A/g, and (D) the relationship between the specific capacitance and current density.

Information (SI) Figure S1A. Further experiment with XPS (SI Figure S1B) displays two binding energy peaks of Mn 2p$^{3/2}$ and Mn 2p$^{1/2}$ centered at 641.9 and 653.6 eV, respectively. The spin energy separation of 11.7 eV vertified that the valence state of the element Mn in the product is Mn^{4+} (IV), which is consistent with our previous report.[37]

Morphological evolution of the CSS upon pencil-drawing and electrodeposition process was studied using SEM. Figure 3A shows that the CSS is composed of irregularly ordered cellulose fibers with a diameter of ca. 20 μm, which is similar to the structure of swollen fibers reported by Park et al.[38] The rough surface of CSS, shown in Figure 3B, could enhance the mechanical exfoliation and adhesion of the graphitic species (Figure 3C) on the surface of CSS. And the drawing of pencil lead on CSS gives rise to multilayer graphite sheets as shown in Figure 3D, inducing continuous conducting paths for the electrodeposition of PEDOT species thereafter. A typical SEM micrograph of PEDOT species (Figure 3E,F) shows that PEDOT fibers with a diameter of ca. 20 nm are entangled with each other, forming porous networks on the graphite-coated CSS membrane. Subsequently, the MnO$_2$ species coated on the CSS/G/PEDOT exhibits uniform nanowire structures, which are highly stacked to form an intercrossed network structure as shown in Figure 3G-H. Furthermore, the homogeneous network sturcture of CSS/G/PEDOT/MnO$_2$ sample is validated by TEM inspection as shown in Figure 3I. And Figure 3J reveals that the diameter of amorphous MnO$_2$ nanowires ranges from 3 to 5 nm. In addition, the EDS analysis (SI Figure S2) indicates the presence of C, S, and Mn

elements in these hybrid electrodes, coresponding to graphite, PEDOT and MnO$_2$ species, respectively.

In order to evaluate the microstructure and electrochemical performance of CSS/G/PEDOT electrodes with different PEDOT deposition conditions, the SEM, CV, galvanostatic charge−discharge, and EIS measurements were conducted; and the results are presented in SI Figures S3 and S4. Apparently, the CSS/G/PEDOT electrode with 5 C PEDOT deposition has the lowest inherent resistance (R_s) value and relatively high electrochemical performance. In the following discussion, the deposition charge of PEDOT is fixed at 5 C.

The electrochemical properties of CSS/G, CSS/G/PEDOT, and CSS/PEDOT/MnO$_2$ with 2 C MnO$_2$ deposition are displayed in Figure 4. Figure 4A shows that the R_s value decreases from 1133 to 4.6 Ω after 5 C electrodepositing of PEDOT on CSS/G. The result indicates that the intermediate PEDOT layer significantly reduces the internal resistance of the electrode, and improves the transportation and collection of electrons within the electrode. The deposition of 2 C MnO$_2$ on CSS/G/PEDOT electrode leads to the slightly increasing of R_s from 4.6 to 5.7 Ω.[39] As shown in Figure 4B, the addition of PEDOT and MnO$_2$ species results in the gradually increasing of CV curves integrate area, corresponding to the increase of capacitance. And the contribution of capacitance from graphite sheets in CSS/G electrode is negligible. Figure 4C shows that after the deposition of MnO$_2$, the galvanostatic charge−discharge curve of CSS/G/PEDOT/MnO$_2$ electrode maintains roughly inverted triangle shape, indicating its highly current efficiency and reversible electrochemical performance.[26] Besides, CSS/G/PEDOT/MnO$_2$ electrode has longer discharge
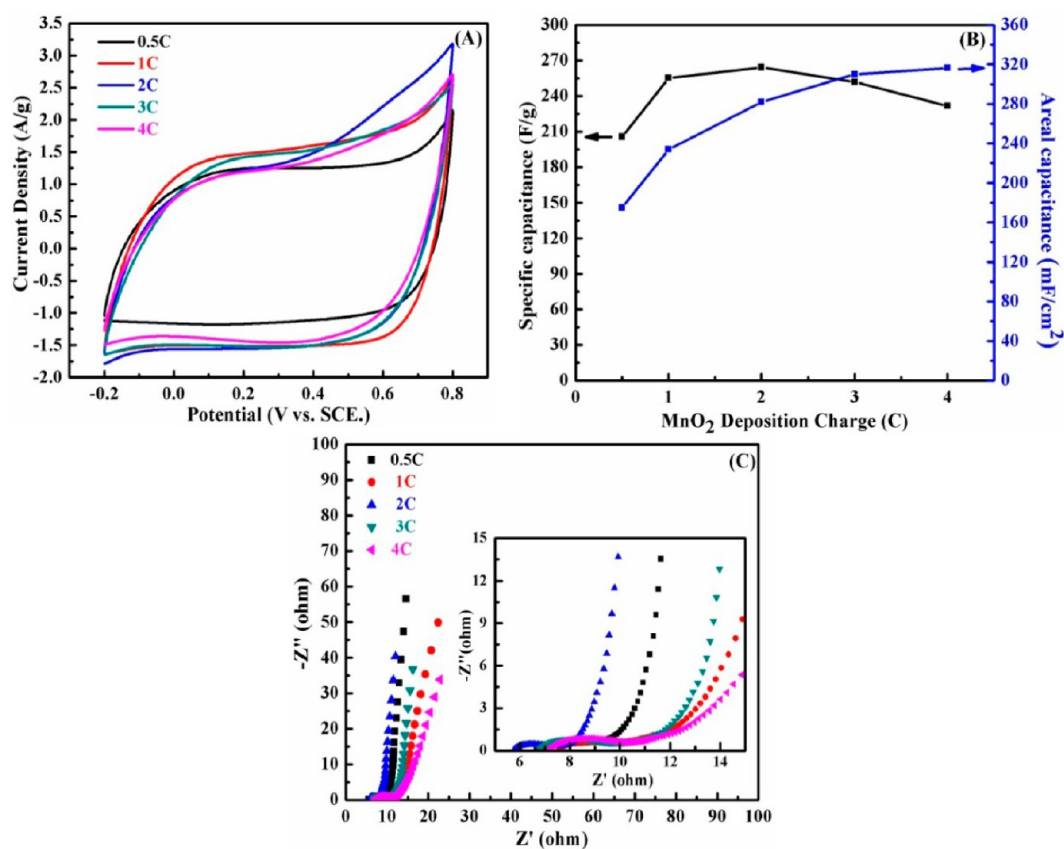
Figure 5. Electrochemical properties of CSS/G/PEDOT/MnO$_2$ electrodes with different MnO$_2$ deposition charge: (A) CV curves at 10 mV/s, (B) specific capacitance, areal capacitance of different electrodes at 10 mV/s, and (C) Nyquist plots.

time than CSS/G/PEDOT electrode. According to eq 1, CSS/G/PEDOT obtains a specific capacitance of 143.7 F/g, while CSS/G/PEDOT/MnO$_2$ (active materials mass loading: 3.3 mg) achieves 195.9 F/g at 0.5 A/g, which is higher than that reported by Cui et al. (12 F/g)[25] and Chou et al. (167.5 F/g at 77 mA/g).[40] When the current density further reaches 10 A/g (Figure 4D), the specific capacitance of CSS/G/PEDOT/MnO$_2$ hybrid electrode decreases to 51 F/g, slightly lower than 88 F/g of CSS/G/PEDOT electrode (active mass loading: 2.3 mg). As the high conductivity of electrode favors rate capability for high power performance and fast charge−discharge;[26] this phenomenon is derived from the relatively poor electrical conductivity of CSS/G/PEDOT/MnO$_2$ hybrid electrode, compared to CSS/G/PEDOT electrode. However, as shown in SI Figure S4C, the value is still higher than 38 F/g of CSS/G/PEDOT electrode with 7C PEDOT deposition charge (active mass loading: 3.3 mg), indicating the advantages of using the ternary composite of graphite, PEDOT, and MnO$_2$ species.

The dependence of MnO$_2$ deposited mass on electrochemical properties of CSS/G/PEDOT/MnO$_2$ electrodes is further systemically investigated, as shown in Figure 5. CV curves of CSS/G/PEDOT/MnO$_2$ hybrid electrodes with varying MnO$_2$ deposition charges at 10 mV/s were presented in Figure 5A. The stimulated current response of unit active material mass gradually increases with the MnO$_2$ deposition charge from 0.5 to 2 C, indicating its improved specific capacitance. As the MnO$_2$ deposition charge further increases to 4 C, the corresponding current density decreases gradually. It is mainly attributed to the low utilization efficiency of active

materials resulting from the compact MnO$_2$ nanowires (Figure 6G).[39] Figure 5B reveals that CSS/G/PEDOT/MnO$_2$ with 2 C MnO$_2$ deposition charge possesses the highest specific capacitance of 264.1 F/g at 10 mV/s, which is comparable with the recent report about CNT@PPy sponge (310 F/g at 20 mV/s).[41] Besides, the fabricated CSS/G/PEDOT/MnO$_2$ electrode with 2 C MnO$_2$ deposition charge is relative lightweight (i.e., total electrode mass loading: 8.0 mg/cm^2), which is lighter than the PANI/Au/paper electrode (14 mg/cm^2) using Au species as intermediate conductive layer.[1] Figure 5B indicates that the areal capacitance of CSS/G/PEDOT/MnO$_2$ (0.5 C: 175 mF/cm^2; 1 C: 234 mF/cm^2; 2 C: 282 mF/cm^2, 3 C: 310 mF/cm^2 and 4 C: 316.4 mF/cm^2) gradually increases with the MnO$_2$ deposition charge from 0.5 to 4 C, and eventually it reaches a maximum value. CSS/G/PEDOT/MnO$_2$ with 4 C MnO$_2$ loading possesses the highest areal capacitance of 316.4 mF/cm^2 at 10 mV/s, which is much higher than multilayered MnO$_2$/Ni/G/Paper (175 mF/cm^2),[26] ordered PANI nanowire array (170 mF/cm^2 at 5 mV/s),[42] and is comparable to PPy-coated paper (420 mF/cm^2)[16] and pencil-drawing G/PANI networks hybrid electrodes (355.6 mF/cm^2 at 0.5 mA/cm^2).[27] Figure 5C shows that the CSS/PEDOT/MnO$_2$ electrode with 2 C MnO$_2$ possesses the lowest R_s among all electrodes, and exhibits a nearly vertical line along the imaginary axis in the low-frequency region, which is consistent with its ideal capacitive behavior.

In order to understand the formation process of MnO$_2$ nanowires, the deposition charges-series analysis of the MnO$_2$ growth process is performed (Figure 6). Figure 6A,B reveals that the MnO$_2$ species initially nucleated on the surface of
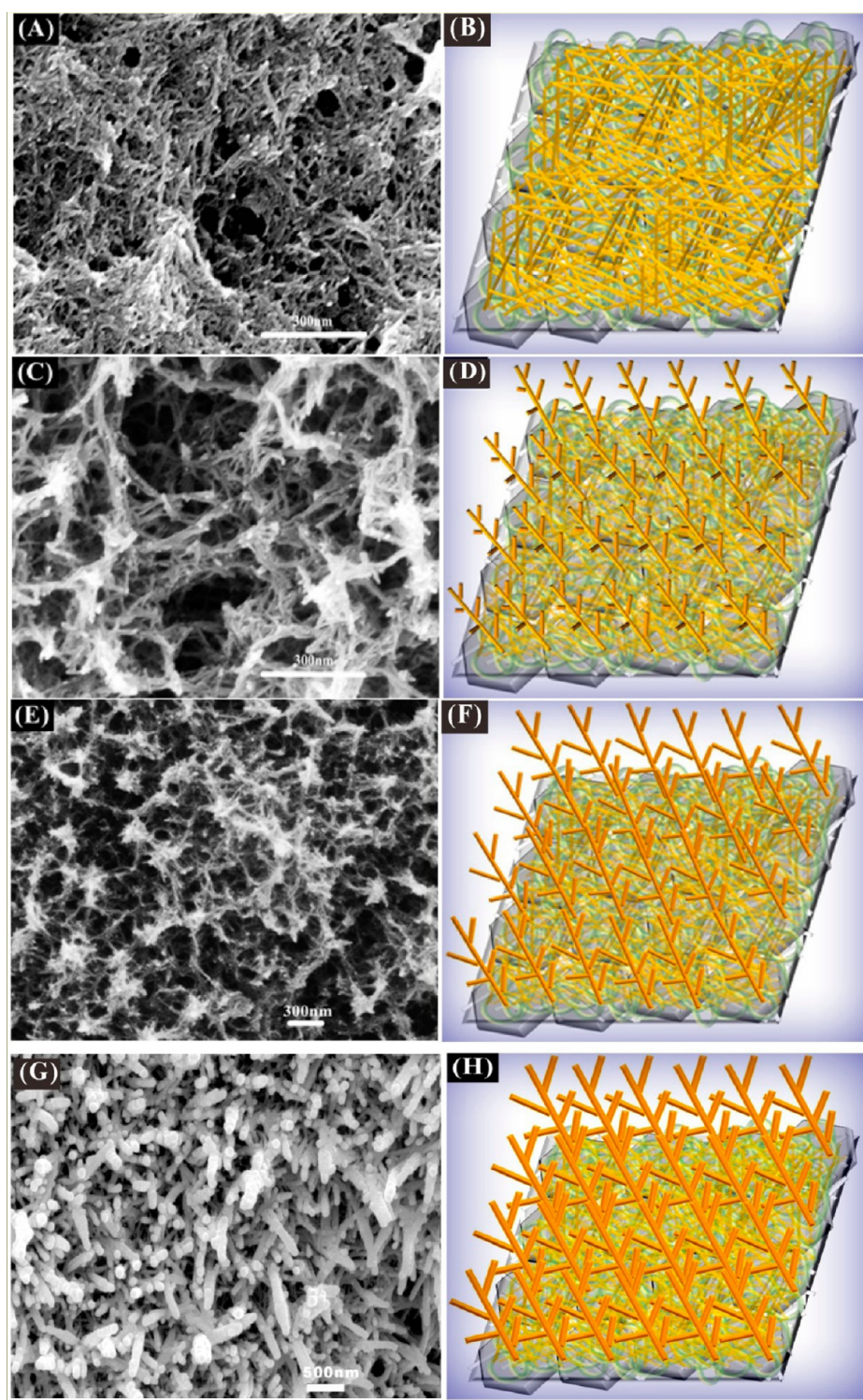
Figure 6. SEM images and corresponding schematic illustration for the MnO_2 nanowires growing on the CSS/G/PEDOT electrode: (A and B) 0.5 C MnO_2 deposition; (C and D) 1 C MnO_2 deposition; (E and F) 2 C MnO_2 deposition; and (G and H) 4 C MnO_2 deposition.

PEDOT to form in-plane horizontal nanowires due to the matched chemical bond between PEDOT and MnO_2 species.[29] As the deposition charges reached 1 C (Figure 6C,D), the MnO_2 species further formed numerous dendrite-like nanowires with few branched nanofibers pointing outward. When the deposition charge increase to 2 C (Figure 6E,F), these branched MnO_2 nanofibers spontaneously grew into intercrossed nanowire networks. Further increasing the MnO_2

deposition charges to 4 C leads to the transverse growth of branched MnO_2 nanofibers (Figure 6G,H). The experimental results reveal that the morphological evaluation of MnO_2 nanowires follows a progressive nucleation mechanisms because the MnO_2 nanowires grew along different directions step-by-step rather than a single direction with the varying of MnO_2 deposition charge.[28] The formation of MnO_2 nanowire networks is attributed to the extraordinarily high surface energy
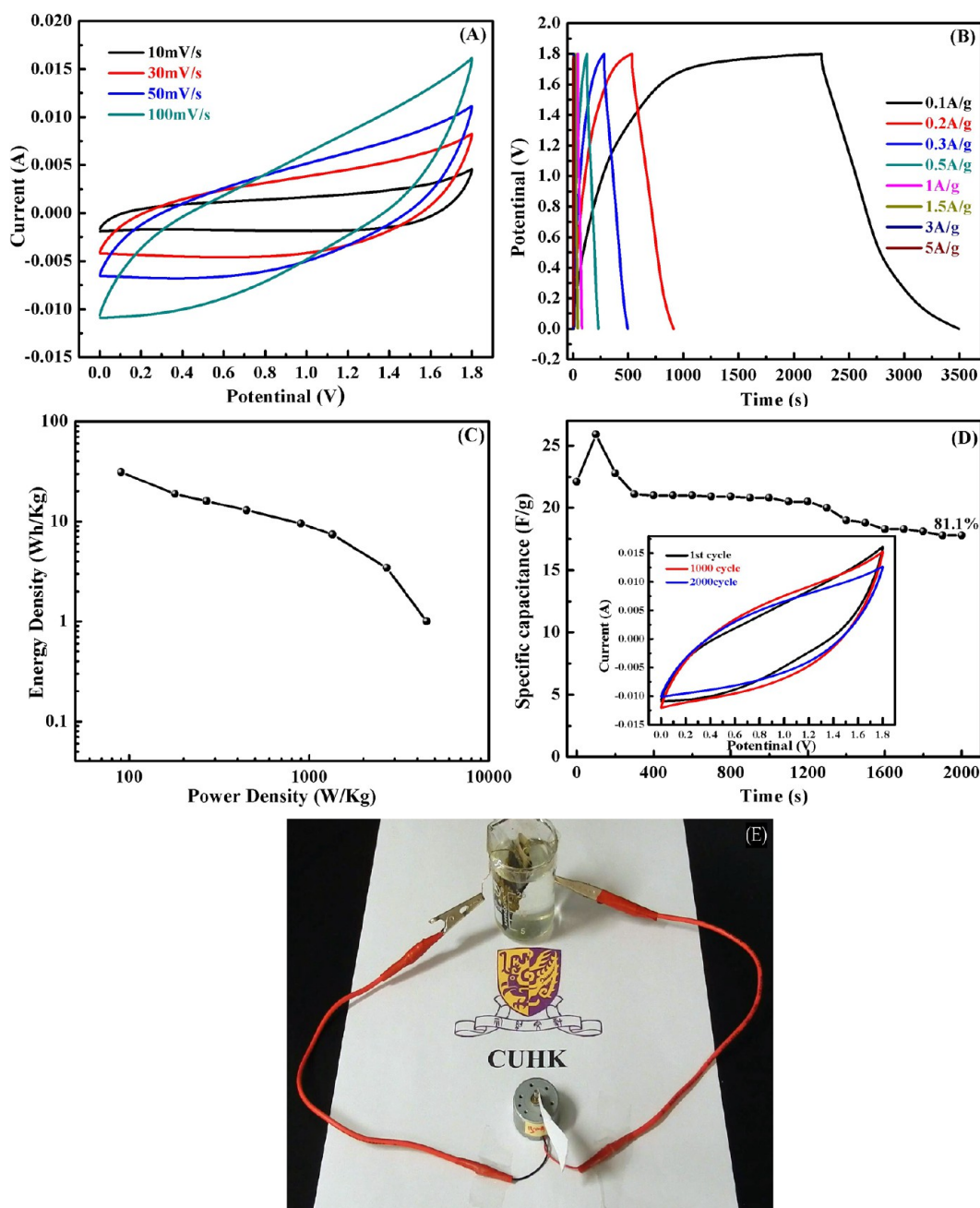
Figure 7. Electrochemical properties of asymmetrical supercapacitor: (A) CV curves at different scan rates, (B) the galvanostatic charge–discharge curves at different current density, (C) the Ragone plot, (D) the life cycle stability at a current density of 1 A/g (with the inset showing the CV curves after 1 cycle, 1000 cycles, and 2000 cycles, respectively), and (E) the digital photogram of a motor driven by an asymmetrical supercapacitor.

of individual nanowires.[43] In order to minimize the overall surface energy, the nanowires could interact spontaneously to form MnO_2 nanowire network structures on the CSS/G/PEDOT electrode. On the basis of the aforementioned analysis of nanowire growth mechanism, the enhanced electrochemical performance of the CSS/G/PEDOT/MnO_2 electrode with 2 C MnO_2 deposition should be derived from its homogeneously network structure: (i) the conductive networks within electrode are well-built because the PEDOT porous layers tightly combined with graphite layers that create electron "superhighways" for charge storage and delivery; (ii) the MnO_2 nanowires composed of 3-D network structure provide efficient diffusion paths for electrolyte ions, which significantly enhance the

intercalation of ions and effective utilization of electrode materials.

To testify to the potential applications for energy storage device, an asymmetric supercapacitor is assembled using the optimized CSS/G/PEDOT/MnO_2 electrode and AC electrode as the positive and negative electrodes (the detailed process is shown in SI Figure S5). The as-prepared asymmetric supercapacitor exhibits an ideal capacitive behavior with approximately rectangular CV curves from 10 to 100 mV/s (Figure 7A) within a potential window of 1.8 V, indicating its excellent power characteristic.[33] Besides, digital photographs of the asymmetric supercapacitor device in different bending states are shown in SI Figure S6. When the supercapacitor is bent by 90° and 180°, no visible changes in CV curves are

observed, which confirms that the device has excellent mechanical flexibility. Galvanostatic discharge curves of the supercapacitor device at various current densities are illustrated in Figure 7B. The charge−discharge curve maintains a relatively good symmetry even at a high current density of 5 A/g, demonstrating its good rate capability. On the basis of these data, Ragone plot of the device describing the relation between energy density and power density is obtained in Figure 7C. It reveals that the asymmetrical supercapacitor can deliver an energy density as high as 31.1 Wh/kg at a power density of 90 W/kg and maintain 1 Wh/kg at a high power density of 4500 W/kg, which exhibits superior performance over MnO_2 nanowire/graphene//graphene (30.4 Wh/kg at 100 W/kg),[33] graphitic hollow carbon spheres/MnO_2//graphitic hollow carbon spheres (22.1 Wh/kg at 100 W/kg)[44] and $Ni(OH)_2$/graphene //RGO (31 Wh/kg at 420 W/kg)[45] and is comparable to $Ni(OH)_2$-CNTs//AC (32.5 Wh/kg at 1800 W/kg),[46] Co_3O_4/PPy/MnO_2//AC (34.3 Wh kg^{-1} at 80.0 Wh/kg),[37] and CoO/PPy//AC (43.5 Wh/kg at 87.5 W/kg).[47] The leakage current and the self-discharge tests of the asymmetric supercapacitor are shown in SI Figure S7, in which the leakage current was stable at about 0.95 mA for a period over 2 h, and the open potential of the device reached about 0.59 V after 24 h. These large leakage current and self-discharge features are probably derived from the cooperation of the high mobility of Na^+ ion in liquid electrolyte and their easy penetrability into the micrometer scale macroporous of the CSS membrane (Figure 3A).[48]

Furthermore, the supercapacitor possesses long-term stability over 2000 cycles at a current density of 1 A/g as shown in Figure 7D. The specific capacitance of the device increased at the beginning of the test due to self-activation process of the device, which implies that more sufficient contacts between electrodes and electrolyte are formed as well as more active sites in the electrode participate in electrochemical reaction.[49] The specific capacitance of the device retains 17.8 F/g after 2000 cycles, corresponding to 81.1% of its initial specific capacitance (20.8 F/g), which is higher than MnO_2 nanowire/graphene//graphene (79% after 1000 cycles),[33] C-PGF//$Ni(OH)_2$/CNTs (78% after 2000 cycles)[50] and Mn_3O_4/graphene nanosheets composites (73% after 1000 cycles).[51] The cycle life of the asymmetric supercapacitor is evidenced by the slightly reduced CV integral area (see the inset of Figure 7D) and the well-maintained nanostructures of the CSS/G/PEDOT/MnO_2 electrode (SI Figure S8) after 2000 cycling tests. In addition, the asymmetric supercapacitor device after 2000 cycles stability test can still drive a mini rotation motor (1.5 V, 49 mW) robustly after 43 s of charging at 5.7 mA (Figure 7E and SI Video S1), demonstrating its potential for energy storage systems. To illustrate the portable properties of the flexible hybrid electrode, a three-supercapacitor tandem device, i.e. symmetrical all-solid-state supercapacitor, also was fabricated to lighten a LED (Figure S9).

4. CONCLUSIONS

The flexible hybrid electrode consisting of a ternary composite, i.e., G/PEDOT/MnO_2, and a cellulose-based CSS membrane is fabricated, which exhibits a high areal capacitance of 316.6 mF/cm^2 at 10 mV/s and specific capacitance of 195.7 F/g at 0.5 A/g. The assembled asymmetrical supercapacitor by CSS/G/PEDOT/MnO_2//AC delivers a high energy density of 31.4 Wh/kg at a power density of 90 W/kg and an acceptable cycling performance of 81.1% retention after 2000 cycles. The

approach represents a promising avenue to fabricate planar asymmetrical supercapacitors with high flexibility and high electrochemical performance because it is low-cost, environmentally benign, and can be scaled-up with ease.

■ ASSOCIATED CONTENT

ⓈSupporting Information

FT-IR and XPS of CSS/G/PEDOT/MnO_2 electrode; X-ray energy dispersive spectrometer (EDS) of a CSS/G/PEDOT/MnO_2 electrode; SEM micrographs of CSS/G/PEDOT electrodes with different PEDOT deposition charges; the electrochemical properties of CSS/G/PEDOT electrodes with different PEDOT deposition charges; the CV curves of CSS/G/PEDOT/MnO_2 hybrid electrode and AC electrode at a scan rate of 50 mV/s; leakage current curve and self-discharge curve of the designed asymmetric supercapacitor device; SEM images of CSS/G/PEDOT/MnO_2 after 2000 cycles test; CV curves of the asymmetric supercapacitor at a scan rate of 100 mV/s when it is bent by 0°, 90°, and 180°; electrochemical properties of all-solid symmetric supercapacitor; and a video. This material is available free of charge via the Internet at http://pubs.acs.org.

■ AUTHOR INFORMATION

Corresponding Author
*E-mail: lizhang@mae.cuhk.edu.hk.

Author Contributions
The manuscript was written through contributions of all authors. All authors have given approval to the final version of the manuscript.

Notes
The authors declare no competing financial interest.

■ ABBREVIATIONS

CSS, commercial supercapacitor separator
G, graphite
XRD, X-ray diffraction
FT-IR, Fourier-transform infrared spectroscopy
XPS, X-ray photoelectron spectroscopy
SEM, field-emission scanning electron microscope
TEM, Transmission electron microscopy

■ REFERENCES

(1) Yuan, L. Y.; Xiao, X.; Ding, T. P.; Zhong, J. W.; Zhang, X. H.; Shen, Y.; Hu, B.; Huang, Y. H.; Zhou, J.; Wang, Z. L. Paper-Based Supercapacitors for Self-Powered Nanosystems. *Angew. Chem., Int. Ed.* **2012**, *124*, 5018−5022.

(2) Cai, X.; Peng, M.; Yu, X.; Fu, Y. P.; Zhou, D. C. Flexible Planar/Fiber-architectured Supercapacitors for Wearable Energy Storage. *J. Mater. Chem. C* **2014**, *2*, 1184−1200.

(3) Miller, J. R.; Simon, P. Electrochemical Capacitors for Energy Management. *Science* **2008**, *321*, 651−652.

(4) Lu, X. H.; Zhai, T.; Zhang, X. H.; Shen, Y. Q.; Yuan, L. Y.; Hu, B.; Gong, L.; Chen, J.; Gao, Y. H.; Zhou, J.; Tong, Y. X.; Wang, Z. L. $WO_{3−x}$@Au@MnO_2 Core-Shell Nanowires on Carbon Fabric for

High-Performance Flexible Supercapacitors. *Adv. Mater.* **2012**, *24*, 938−944.

(5) Qin, Y.; Wang, X.; Wang, Z. L. Microfibre−Nanowire Hybrid Structure for Energy Scavenging. *Nature* **2008**, *451*, 809−813.

(6) Wang, K.; Meng, Q. H.; Zhang, Y. J.; Wei, Z. X.; Miao, M. H. High-Performance Two-Ply Yarn Supercapacitors Based on Carbon Nanotubes and Polyaniline Nanowire Arrays. *Adv. Mater.* **2013**, *25*, 1494−1498.

(7) Li, Y. Y.; Li, Z. S.; Shen, P. K. Simultaneous Formation of Ultrahigh Surface Area and Three-Dimensional Hierarchical Porous Graphene-Like Networks for Fast and Highly Stable Supercapacitors. *Adv. Mater.* **2013**, *25*, 2474−2480.

(8) Cheng, Y. W.; Lu, S. T.; Zhang, H. B.; Varanasi, C.; Liu, J. Synergistic Effects from Graphene and Carbon Nanotubes Enable Flexible and Robust Electrodes for High-performance Supercapacitors. *Nano Lett.* **2012**, *12*, 4206−4211.

(9) Rakhi, R. B.; Chen, W.; Cha, D. K.; Alshareef, H. N. Substrate Dependent Self-Organization of Mesoporous Cobalt Oxide Nanowires with Remarkable Pseudocapacitance. *Nano Lett.* **2012**, *12*, 2559−2567.

(10) Jiang, J.; Li, Y. Y.; Liu, J.; Huang, X. T.; Yuan, C. Z.; Lou, X. W. Recent Advances in Metal Oxide-Based Electrode Architecture Design for Electrochemical Energy Storage. *Adv. Mater.* **2012**, *24*, 5166−5180.

(11) Nyholm, L.; Nyström, G.; Mihranyan, A.; Strømme, M. Toward Flexible Polymer and Paper-Based Energy Storage Devices. *Adv. Mater.* **2011**, *23*, 3751−3769.

(12) Zhang, G. Q.; Wu, H. B.; Hoster, H. E.; Chan-Park, M. B.; Lou, X. W. Single-Crystalline NiCo$_2$O$_4$ Nanoneedle Arrays Grown on Conductive Substrates as Binder-Free Electrodes for High-Performance Supercapacitors. *Energy Environ. Sci.* **2012**, *5*, 9453−9456.

(13) Peng, L. L.; Peng, X.; Liu, B. R.; Wu, C. Z.; Xie, Y.; Yu, G. H. Ultrathin Two-Dimensional MnO$_2$/Graphene Hybrid Nanostructures for High-Performance, Flexible Planar Supercapacitors. *Nano Lett.* **2013**, *13*, 2151−2157.

(14) Yoo, J. J.; Balakrishnan, K.; Huang, J. S.; Meunier, V.; Sumpter, B. G.; Srivastava, A.; Conway, M.; Reddy, A.L. M.; Yu, J.; Vajtai, R.; Ajayan, P. M. Ultrathin Planar Graphene Supercapacitors. *Nano Lett.* **2011**, *11*, 1423−1427.

(15) Gwon, H.; Kim, H. S.; Lee, K. U.; Seo, D. H.; Park, Y. C.; Lee, Y. S.; Ahn, B. T.; Kang, K. S. Flexible Energy Storage Devices Based on Graphene Paper. *Energy Environ. Sci.* **2011**, *4*, 1277−1283.

(16) Yuan, L. Y.; Yao, B.; Hu, B.; Huo, K. F.; Chen, W.; Zhou, J. Polypyrrole-Coated Paper for Flexible Solid-State Energy Storage. *Energy Environ. Sci.* **2013**, *6*, 470−476.

(17) Niu, Z. Q.; Zhang, L.; Liu, L. L.; Zhu, B. W.; Dong, H. B.; Chen, X. D. All-Solid-State Flexible Ultrathin Micro-Supercapacitors Based on Graphene. *Adv. Mater.* **2013**, *25*, 4035−4042.

(18) Zhang, Z. S.; Wang, W.; Li, C.; Wei, L.; Chen, X. J.; Tong, Y. X.; Mai, K. C.; Lu, X. H. Highly Conductive Ethylene-Vinyl Acetate Copolymer/carbon Nanotube Paper for Lightweight and Flexible Supercapacitors. *J. Power Sources* **2014**, *248*, 1248−1255.

(19) Yu, Z. N.; Duong, B.; Abbitt, D.; Thomas, J. Highly Ordered MnO$_2$ Nanopillars for Enhanced Supercapacitor Performance. *Adv. Mater.* **2013**, *25*, 3302−3306.

(20) Wang, X.; Sumboja, A.; Foo, W. L.; Yan, C. Y.; Tsukagoshi, K.; Lee, P. S. Rational Design of a High Performance All Solid State Flexible Micro-supercapacitor on Paper. *RSC Adv.* **2013**, 15827−15833.

(21) Kang, Y. J.; Chung, H.; Han, C. H.; Kim, W. All-Solid-State Flexible Supercapacitors based on Papers Coated with Carbon Nanotubes and Ionic-Liquid-Based Gel Electrolytes. *Nanotechnology* **2012**, *23*, 065401.

(22) Jiang, W.; Zhang, K.; Wei, L.; Yu, D.; Wei, J.; Chen, Y. Hybrid Ternary Rice Paper-Manganese Oxide-Carbon Nanotube Nanocomposites for Flexible Supercapacitors. *Nanoscale* **2013**, *5*, 11108−11117.

(23) Wang, X.; Gao, K.; Shao, Z.; Peng, X.; Wu, X.; Wang, F. Layer-by-Layer Assembled Hybrid Multilayer Thin Film Electrodes based on Transparent Cellulose Nanofibers Paper for Flexible Supercapacitors Applications. *J. Power Sources* **2014**, *249*, 148−155.

(24) Hu, L.; Wu, H.; Cui, Y. Printed Energy Storage Devices by Integration of Electrodes and Separators into Single Sheets of Paper. *Appl. Phys. Lett.* **2010**, *96*, 183502.

(25) Zheng, G.; Hu, L.; Wu, H.; Xie, X.; Cui, Y. Paper Supercapacitors by a Solvent-Free Drawing Method. *Energy Environ. Sci.* **2011**, *4*, 3368−3373.

(26) Feng, J. X.; Li, Q.; Lu, X. F.; Tong, Y. X.; Li, G. R. Flexible Symmetrical Planar Supercapacitors Based on Multi-Layered MnO$_2$/Ni/Graphite/Paper Electrodes with High-Efficient Electrochemical Energy Storage. *J. Mater. Chem. A* **2014**, *2*, 2985−2992.

(27) Yao, B.; Yuan, L. Y.; Xiao, X.; Zhang, J.; Qi, Y. Y.; Zhou, J.; Hu, B.; Chen, W. Paper-Based Solid-State Supercapacitors with Pencil-Drawing Graphite/Polyaniline Networks Hybrid Electrodes. *Nano Energy* **2013**, *2*, 1071−1078.

(28) Wei, W. F.; Cui, X. W.; Mao, X. H.; Chen, W. X.; Ivey, D. G. Morphology Evolution in Anodically Electrodeposited Manganese Oxide Nanostructures for Electrochemical Supercapacitor Applications-Effect of Supersaturation Ratio. *Electrochim. Acta* **2011**, *56*, 1619−1628.

(29) Guo, C. X.; Wang, M.; Chen, T.; Lou, X. W.; Li, C. M. A Hierarchically Nanostructured Composite of MnO$_2$/Conjugated Polymer/Graphene for High-Performance Lithium Ion Batteries. *Adv. Energy Mater.* **2011**, *1*, 736−741.

(30) Huang, J. Y.; Wang, K.; Wei, Z. X. Conducting Polymer Nanowire Arrays with Enhanced Electrochemical Performance. *J. Mater. Chem.* **2010**, *20*, 1117−1121.

(31) Tang, P. Y.; Zhao, Y. Q.; Wang, Y. M.; Xu, C. L. A Metal-Decorated Nickel Foam-inducing Regulatable Manganese Dioxide Nanosheet Array Architecture for High-Performance Supercapacitor Applications. *Nanoscale* **2013**, *5*, 8156−8163.

(32) Tang, P. Y.; Zhao, Y. Q.; Xu, C. L. Step-by-Step Assembled Poly (3, 4-ethylenedioxythiophene)/Manganese Dioxide Composite Electrodes: Tuning the Structure for High Electrochemical Performance. *Electrochim. Acta* **2013**, *89*, 300−309.

(33) Wu, Z. S.; Ren, W.; Wang, D. W.; Li, F.; Liu, B.; Cheng, H. M. High-Energy MnO$_2$ Nanowire/Graphene and Graphene Asymmetric Electrochemical Capacitors. *ACS Nano* **2010**, *4*, 5835−5842.

(34) Okita, Y.; Saito, T.; Isog, A. Entire Surface Oxidation of Various Cellulose Microfibrils by TEMPO-Mediated Oxidation. *Biomacromolecules* **2010**, *11*, 1696−1700.

(35) Eichhorn, S. J. Cellulose Nanowhiskers: Promising Materials for Advanced Applications. *Soft Matter* **2011**, *7*, 303−315.

(36) Chen, Y. C.; Hsu, Y. K.; Lin, Y. G.; Lin, Y. K.; Horng, Y. Y.; Chen, L. C.; Chen, K. H. Highly Flexible Supercapacitors with Manganese Oxide Nanosheet/Carbon Cloth Electrode. *Electrochim. Acta* **2011**, *56*, 7124−7130.

(37) Han, L. J.; Tang, P. Y.; Zhang, L. Hierarchical Co$_3$O$_4$@PPy@ MnO$_2$ Core−Shell−Shell Nanowire Arrays for Enhanced Electrochemical Energy Storage. *Nano Energy* **2014**, *7*, 42−51.

(38) Park, M. W.; Im, J. K.; Shin, M. K.; Min, Y. H.; Park, J.; Cho, H.; Park, S. J.; Shim, M. B.; Jeon, S. H.; Chung, D. Y.; Bae, J. H.; Park, J. J.; Jeong, U. Y.; Kim, K. N. Highly Stretchable Electric Circuits From a Composite Material of Silver Nanoparticles and Elastomeric Fibres. *Nat. Nanotechnol.* **2012**, *7*, 803−809.

(39) Toupin, M.; Brousse, T.; Bélanger, D. Charge Storage Mechanism of MnO$_2$ Electrode Used in Aqueous Electrochemical Capacitor. *Chem. Mater.* **2004**, *16*, 3184−3190.

(40) Chou, S. L.; Wang, J. Z.; Chew, S. Y.; Liu, H. K.; Dou, S. X. Electrodeposition of MnO$_2$ Nanowires on Carbon Nanotube Paper as Free-Standing, Flexible Electrode for Supercapacitors. *Electrochem. Commun.* **2008**, *10*, 1724−1727.

(41) Li, P. X.; Shi, E. Z.; Yang, Y. B.; Shang, Y. Y.; Peng, Q.; Wu, S. T.; Wei, J. Q.; Wang, K. L.; Zhu, H. W.; Yuan, Q.; Cao, A. Y.; Wu, D. H. Carbon Nanotube−Polypyrrole Core−Shell Sponge and Its Application as Highly Compressible Supercapacitor Electrode. *Nano Res.* **2014**, *7*, 209−218.

(42) Wang, K.; Wu, H. P.; Meng, Y. N.; Zhang, Y. J.; Wei, Z. X. Integrated Energy Storage and Electrochromic Function in One

Flexible Device: An Energy Storage Smart Window. *Energy Environ. Sci.* **2012**, *5*, 8384−8389.

(43) Wu, L. C.; Chen, Y. J.; Mao, M. L.; Li, Q. H.; Zhang, M. Facile Synthesis of Spike-Piece-Structured Ni(OH)$_2$ Interlayer Nanoplates on Nickel Foam as Advanced Pseudocapacitive Materials for Energy Storage. *ACS Appl. Mater. Interfaces* **2014**, DOI: 10.1021 /am500449b.

(44) Lei, Z. B.; Zhang, J. T.; Zhao, X. S. Ultrathin MnO$_2$ Nanofibers Grown on Graphitic Carbon Spheres as High-performance Asymmetric Supercapacitor Electrodes. *J. Mater. Chem.* **2012**, *22*, 153−160.

(45) Wang, H. L.; Liang, Y. Y.; Mirfakhrai, T.; Chen, Z.; Casalongue, H. S.; Dai, H. J. Advanced Asymmetrical Supercapacitors Based on Graphene Hybrid Materials. *Nano Res.* **2011**, *4*, 729−736.

(46) Tang, Z.; Tang, C. H.; Gong, H. A High Energy Density Asymmetric Supercapacitor from Nano-architectured Ni (OH)$_2$/Carbon Nanotube Electrodes. *Adv. Funct. Mater.* **2012**, *22*, 1272−1278.

(47) Zhou, C.; Zhang, Y. W.; Li, Y. Y.; Liu, J. P. Construction of High-Capacitance 3D CoO@Polypyrrole Nanowire Array Electrode for Aqueous Asymmetric Supercapacitor. *Nano Lett.* **2013**, *13*, 2078−2085.

(48) He, Y. M.; Chen, W. J.; Zhou, J. Y.; Li, X. D.; Tang, P. Y.; Zhang, Z. X.; Fu, J. C.; Xie, E. Q. Constructed Uninterrupted Charge-Transfer Pathways in Three-Dimensional Micro/Nanointerconnected Carbon-Based Electrodes for High Energy-Density Ultralight Flexible Supercapacitors. *ACS Appl. Mater. Interfaces* **2014**, *6*, 210−218.

(49) Lu, X. H.; Zheng, D. Z.; Zhai, T.; Liu, Z. Q.; Huang, Y. Y.; Xie, S. L.; Tong, Y. X. Facile Synthesis of Large-Area Manganese Oxide Nanorod Arrays as a High-Performance Electrochemical Supercapacitor. *Energy Environ. Sci.* **2011**, *4*, 2915−2921.

(50) Long, C. L.; Wei, T.; Yan, J.; Jiang, L. L.; Fan, Z. J. Supercapacitors Based on Graphene-Supported Iron Nanosheets as Negative Electrode Materials. *ACS Nano* **2013**, *7*, 11325−11332.

(51) Zhang, W. F.; Liu, F.; Li, Q. Q.; Shou, Q. L.; Cheng, J. P.; Zhang, L.; Nelson, B. J.; Zhang, X. B. Transition Metal Oxide and Graphene Nanocomposites for High-performance Electrochemical Capacitors. *Phys. Chem. Chem. Phys.* **2012**, *14*, 16331−16337.